



# Soft Sensors for Property-Controlled Multi-Stage Press Hardening of 22MnB5

Juri Martschin<sup>1</sup> · Malte Wrobel<sup>2</sup> · Joshua Grodotzki<sup>1</sup> · Thomas Meurer<sup>2</sup> · A. Erman Tekkaya<sup>1</sup>

Received: 7 December 2022 / Accepted: 20 July 2023 / Published online: 8 September 2023  
© The Author(s) 2023

## Abstract

In multi-stage press hardening, the product properties are determined by the thermo-mechanical history during the sequence of heat treatment and forming steps. To measure these properties and finally to control them by feedback, two soft sensors are developed in this work. The press hardening of 22MnB5 sheet material in a progressive die, where the material is first rapidly austenitized, then pre-cooled, stretch-formed, and finally die bent, serves as the framework for the development of these sensors. To provide feedback on the temporal and spatial temperature distribution, a soft sensor based on a model derived from the Dynamic mode decomposition (DMD) is presented. The model is extended to a parametric DMD and combined with a Kalman filter to estimate the temperature (-distribution) as a function of all process-relevant control variables. The soft sensor can estimate the temperature distribution based on local thermocouple measurements with an error of less than 10 °C during the process-relevant time steps. For the online prediction of the final microstructure, an artificial neural network (ANN)-based microstructure soft sensor is developed. As part of this, a transferable framework for deriving input parameters for the ANN based on the process route in multi-stage press hardening is presented, along with a method for developing a training database using a 1-element model implemented with LS-Dyna and utilizing the material model Mat248 (PHS\_BMW). The developed ANN-based microstructure soft sensor can predict the final microstructure for specific regions of the formed and hardened sheet in a time span of far less than 1 s with a maximum deviation of a phase fraction of 1.8 % to a reference simulation.

**Keywords** Press hardening · Property control · Soft sensor · Artificial neuronal network · Dynamic mode decomposition

## Abbreviations

ANN Artificial neuronal network  
BDC Bottom dead center

DC Direct current  
DMD Dynamic mode decomposition  
FEM Finite element method  
SVD Singular value decomposition  
TDC Top dead center

---

✉ Juri Martschin  
Juri.Martschin@iul.tu-dortmund.de

Malte Wrobel  
malte.wrobel@kit.edu

Joshua Grodotzki  
Joshua.Grodotzki@iul.tu-dortmund.de

Thomas Meurer  
thomas.meurer@kit.edu

A. Erman Tekkaya  
Erman.Tekkaya@iul.tu-dortmund.de

<sup>1</sup> Institute of Forming Technology and Lightweight Components, TU Dortmund University, Baroper Str. 303, 44227 Dortmund, Germany

<sup>2</sup> Institute of Mechanical Process Engineering and Mechanics, Karlsruhe Institute of Technology (KIT), Hertzstr. 16, 76187 Karlsruhe, Germany

## 1 Introduction

Press hardening of sheet metal in multi-stage dies allows for the production of geometrically complex, hardened components in large batch sizes [1]. For example, the hot shearing and hardening of automotive seat belt buckles [2] and gear parts [3] can be implemented in progressive dies. However, even in conventional single-stage press hardening, predicting the thermal and mechanical interactions, and thus the resulting product properties, is challenging. Achieving zero defect production remains a major challenge [4]. In the case of multi-stage press hardening, the modeling effort required to determine a functional process window

increases considerably [5], and greater uncertainties in the prediction of product properties are given by a multi-step error propagation and an extended disturbance collective. Sources of disturbance include measurement uncertainties of sensors, actuator errors, a variance in the properties of the semi-finished product (e.g. the sheet thickness), and model errors. To compensate for these uncertainties as well as the disturbances and thus implement robust production, closed-loop control can be added to forming processes [6].

First approaches to control spring back [7] or strength [8] in multi-stage hot sheet bending in a progressive die have already been developed. However, the implementation of a comprehensive property control in multi-stage press hardening, i.e., a multivariable control of hardness and geometry features, is still missing. Controlling the product properties requires that the latter are accessed online and fed back during the ongoing process. However, in-situ measurement of properties such as hardness has so far been possible only to a limited extent in such forming processes. For example, with the established 3MA sensor [9], which evaluates micro-magnetic effects such as Barkhausen noise, hardness measurements can only be carried out after the formed component has cooled down. This results in undesirably long idle times when such a sensor is utilized for closed-loop control. Even the in-situ measurement of the spatial and temporal temperature distribution is a challenge itself because in the closed die the temperature can only be recorded at isolated measuring points. To date, the temperature distribution is measured with thermal imaging cameras before the die is closed and after it is opened to estimate whether sufficient cooling below the martensite finish temperature was achieved [10]. The latter, however, does not provide any information on the exact spatial-temporal temperature profile in the sheet, which is particularly important for predicting mixed microstructures for tailored components.

With a so-called soft sensor, a model processing representative measurement variables can be used to infer a target variable [11], which may not be directly measurable with conventional measurement methods. Bambach et al. [12] developed an artificial neural network-based soft sensor for property control in close-die forging, which estimates the grain size evolution in the workpiece dependent on temperature measurements and other forming parameters. Stebner et al. [13] designed a soft sensor for property control in free-form bending relying on an extended Kalman filter capable of predicting local strength and residual hoop stress based on inline hardness measurements.

In the context of this work, the development of soft sensors for the determination of the spatial and temporal temperature distribution as well as for the determination of the final microstructure are presented. The underlining goal is to contribute to the implementation of property-controlled multi-stage press hardening by providing suitable sensors.

First, in Sect. 2 the underlying multi-stage press hardening process and the general control concept are explained. Then, in Sect. 3, a temperature soft sensor is developed based on the dynamic mode decomposition. Subsequently, in Sect. 4, the development of a microstructure soft sensor based on an artificial neural network is presented. Additionally, in Sect. 5, a short motivation is given on how the output of the developed sensors can be further utilized.

## 2 Demo Process and Control Concept

To establish a property control mechanism, multi-stage press hardening in a progressive die (refer to Fig. 1), which is installed in a servo press, is set to be the framework. The overall aim is to control the product properties based on the microstructure, such as hardness, while simultaneously keeping the geometry constant. The material used is uncoated 22MnB5 slit strip with a cross-section of  $2 \times 200$  mm and the chemical composition is given in Table 1. A microstructural analysis of the material according

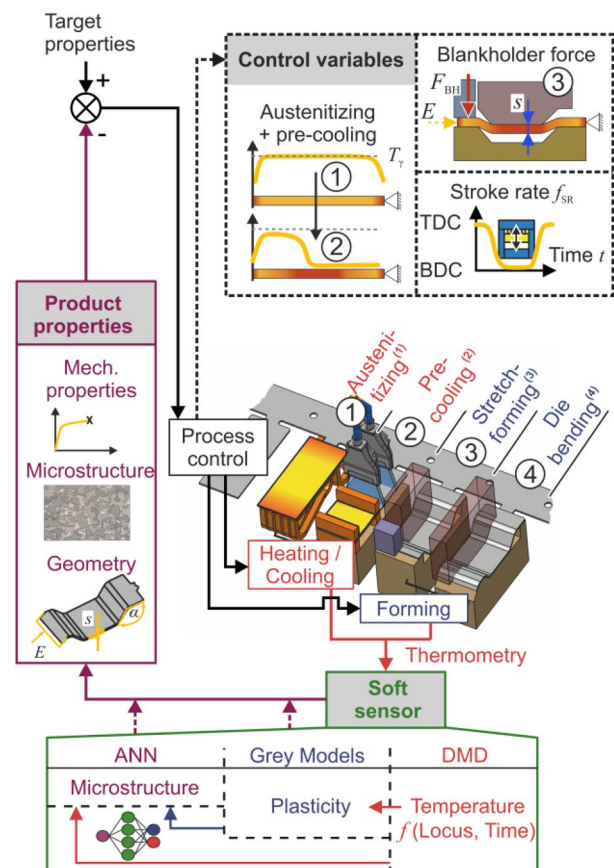


**Fig. 1** Demo process with control loop, control variables, soft sensors, and product properties for property-controlled multi-stage press hardening in the progressive die

**Table 1** Chemical composition of the 22MnB5 slit strip according to the melt analysis

Element (wt%)	Fe 97.935	Mn 1.13	Si 0.33	Cr 0.27	C 0.19	Al 0.036
Element (wt%)	Ni 0.03	Ti 0.028	Cu 0.02	P 0.01	Mo 0.004	N 0.0037
Element (wt%)	As 0.003	S 0.003	B 0.0023	V 0.002	Sn 0.002	Nb 0.001

to DIN EN ISO 643:2013.05 indicates that the base material consists of 70% ferrite, 22% sorbite, 5% pearlite, and 3% fine carbides. The average ferrite grain size  $G_F$  is 12  $\mu\text{m}$ .

During the initial forming stages of the unillustrated progressive die, the slit strip is pre-cut into rectangular blanks (with dimensions of  $W \times L$ : 60 mm  $\times$  140 mm), which are connected to the remaining material for a transfer through the die. In the first stage under consideration for property control, the blank is inductively heated to the austenitizing temperature  $T_\gamma$ . For this purpose, a two-part coil arrangement [14] is built into the progressive die, which allows the sheet blank to be heated to the austenitizing temperature, while the ram is at the bottom dead center (BDC) at a heating rate  $r_h$  of 300 K/s to ensure sufficient stroke rates. In conventional press hardening, the blanks are heated to austenitizing temperatures between 870 °C and 950 °C in the furnace. Due to the high heating rates presented above, the  $A_{C3}$ -temperature increases [15], hence, austenitizing temperatures above 1000 °C are required to achieve a completely homogeneous austenitization while maintaining short holding times. In the second stage, known as the pre-cooling stage, a temperature profile is set along the length of the blank using flat fan nozzles, which partially cool the blank with compressed air, and a DC power source, which partially maintains or raises the sheet temperature through resistance heating. This allows the temperature-dependent flow of the material in the subsequent stages as well as the initial thermal history to be pre-controlled. In the third stage, the first forming stage, a hat-shaped profile is stretch-formed. During stretch-forming, the blank holder force  $F_{BH}$  can be adapted for setting the sheet indentation  $E$  and thus the thickness distribution  $s$ . Finally, during die bending, one side wall of the hat-shaped profile is bent and the resulting profile is calibrated. In both stretch forming and die bending, the formed blank is quenched by contact with actively cooled dies during the holding phase of the ram at BDC. The holding time at BDC is scaled by adjusting the stroke rate  $f_{SR}$  (with constant punch speed) of the servo press, thus the total amount of transmitted thermal energy during the multi-stage process is altered.

During the process, the temperature is measured at different spots using thermocouples installed in the dies and with pyrometers. In addition, the temperature distribution in the sheet is recorded by a thermal imaging camera during

transport with the dies open with the ram at the top dead center (TDC) position. The measured temperature (distribution) is evaluated by a cascade of soft sensors, which predict the product properties on this basis. The latter are compared with predefined target properties so that the process control adjusts the process control variables ( $f_{SR}$ ,  $T_\gamma$ , temperature profile in the second stage,  $F_{BH}$ ) accordingly.

The soft sensor cascade starts with a temperature soft sensor, employing a model-based state observer). This sensor predicts the temporal and spatial temperature distribution using data from temperature sensors. The model used for the temperature soft sensors is elaborated in Sect. 3. Based on the temperature distribution, the strain distribution in the formed sheet is calculated. The latter is not discussed in this paper. However, it should be noted that for efficiently calculating plasticity, a data-based model, employing a similar approach as described in Sect. 3, could be selected. Additionally, Lafarge et al. [16] presented the development of an artificial neural network that could be employed. Finally, by considering the temperature and plasticity calculations, the final microstructure is predicted (see Sect. 4), serving as the foundation for determining the product properties.

### 3 Temperature Soft Sensor Based on Dynamic Mode Decomposition

In order to determine the temperature distribution  $T(\theta, x, t)$  in the sheet across all tool stages of the progressive die for different sets of process parameters  $\theta$ , a multi-stage process is simulated using the finite element code LS-Dyna (solver: R12.0.0). The modeling approach for each process stage follows the setup detailed in Sect. 4.4. The meshed blank, in which the spatial positions of nodes change over time, is depicted in Fig. 2. The left side of the figure shows the mesh of the undeformed blank at the start of the process and the right side depicts the mesh at the end of the forming process. Gray nodes indicate positions for fixture elements, which are irrelevant to the forming process. On the other hand, the red and green nodes are crucial. For simplicity, only the temperatures of the green nodes are considered in the subsequent analysis, as the temperatures exhibit minimal changes in the  $x$ -direction.

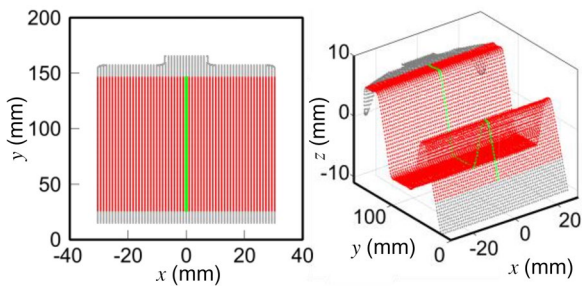


Fig. 2 Mesh before (left) and mesh at the end of the forming process (right)

With these data, in Sect. 3.1 a reduced order system model using dynamic mode decomposition (DMD) is derived. This model is further extended to a parametric DMD in Sect. 3.2, and subsequently, a temperature estimator is developed in Sect. 3.3. The methodology described in Sects. 3.1 to 3.3 can be applied in a similar manner to the temperature output of other finite element programs. For consistency with the other developments presented in Sect. 4, LSDyna is selected in this study.

### 3.1 Dynamic Mode Decomposition

The DMD is a data-driven model order reduction technique that extracts the most important dynamic characteristics from measured or simulated data [17]. It also determines a linear model for the temporal evolution of these modes. For the actual evaluation, simulated data is used, which is summarized in the data vector  $T_{Sim}(t_k)$ , collected at discrete time points  $t_k = (k - 1) \Delta t$  with  $k = 1, 2, \dots, m$ .  $T_{Sim}(t_k)$  denotes the sampled temperatures obtained from the detailed LS-Dyna simulation at the  $n = 119$  most relevant (marked in green) nodes of the sheet metal, as shown in Fig. 2, passing through the three consecutive processing stages: 2 (pre-cooling), 3 (stretch-forming), and 4 (die bending), as depicted in Fig. 1. Figure 3 illustrates the evolution of temperatures  $T_{Sim}(t_k)$  at the nodes marked in green for one set of parameters, demonstrating the range of histories.

$X_1 = [T_{Sim}(t_0) \ T_{Sim}(t_1) \ \dots \ T_{Sim}(t_{m-2})] \in \mathbb{R}^{n \times (m-1)}$  and  $X_2 = [T_{Sim}(t_1) \ T_{Sim}(t_2) \ \dots \ T_{Sim}(t_{m-1})] \in \mathbb{R}^{n \times (m-1)}$  are the snapshot matrices, which are required for the DMD algorithm. The processing time  $t_e$  and the sampling time  $\Delta t$  determine the number of time steps  $m = t_e / \Delta t$ . The DMD assumes that  $T_{Sim}(t_k)$  and  $T_{Sim}(t_{k+1})$  are approximately related by a linear operator  $A \in \mathbb{R}^{n \times n}$ , which yields  $T(t_{k+1}) \approx A T(t_k)$  with the DMD state vector  $T(t_k)$ . This is equivalent to  $X_2 \approx AX_1$  in terms of the snapshot matrices. A least-squares solution  $A$  is obtained by the minimization of the Frobenius norm of  $\|X_2 - AX_1\|$ , which leads to  $A = X_2 X_1^\dagger$ . Here,  $X_1^\dagger$  is the pseudoinverse of  $X_1$ , which can be calculated efficiently using the singular value decomposition (SVD). Furthermore, a

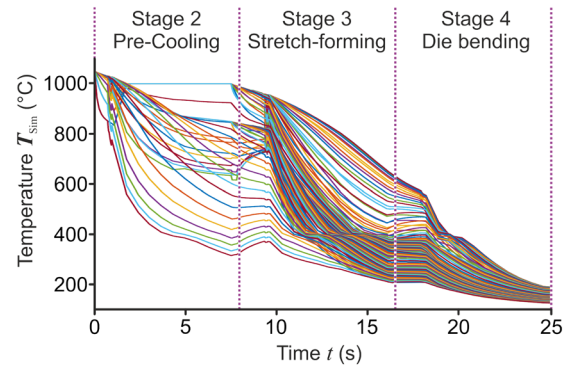


Fig. 3 Temperature evolution in green nodes over the three simulated stages at one specific parameter set

reduced-order representation  $A_r$  of  $A$  can be determined this way. The rank- $r$  truncated DMD is calculated with the following steps [17]:

(1) The rank- $r$  truncated SVD  $X_1 \approx U_r S_r V_r^*$  with  $U_r \in \mathbb{C}^{n \times r}$ ,  $S_r \in \mathbb{C}^{r \times r}$  and  $V_r \in \mathbb{C}^{m \times r}$  is evaluated, where  $*$  denotes the complex conjugate transpose.

(2) The matrix  $A$  is determined using the SVD with  $A = X_2 X_1^\dagger \approx X_2 V_r S_r^{-1} U_r^* = \bar{A}$ . This gives  $T(t_{k+1}) \approx \bar{A} T(t_k)$  to approximate the evolution of the temperature (state) vectors.

The linear transformation  $T_r(\bullet) = U_r^* T(\bullet)$  with  $T_r \in \mathbb{R}^r$  for  $r \ll n$  is introduced to obtain

$$T_r(t_{k+1}) = A_r T_r(t_k) \tag{1}$$

with the reduced order dynamic matrix  $A_r = U_r^* \bar{A} U_r = U_r^* X_2 V_r S_r^{-1}$ .

(3) The eigenvalues of  $\bar{A}$  are summarized in the diagonal matrix  $\Lambda$ , which is derived via the eigendecomposition  $A_r W = \Lambda A_r$ . The related eigenvectors, the DMD modes, are determined by the columns of  $\Phi = X_2 V_r S_r^{-1} W$ .

The discrete-time eigenvalues  $\lambda_k$  are transformed to continuous time ones with  $\omega_k = \ln(\lambda_k) / \Delta t$  [17]. The approximate solution of Eq. (1) for any time  $t$  is then given by

$$T(t) \approx \Phi e^{\Omega t} b \tag{2}$$

With the DMD modes  $\Phi$ , the diagonal matrix  $\Omega$  with eigenvalues  $\omega_k$ , and the vector  $b = \Phi^\dagger T(0)$ .

The sampling time  $\Delta t = 0.01$  s and truncation rank  $r = 50$  are chosen to obtain numerical stability of the reduced order system taking into account the work of Ref. [18]. The results depicted in Fig. 4 are achieved by simulating the DMD model via Eq. (2). In Fig. 4 (top) the time evolution of the average temperature of all nodes  $\text{mean}(T) = \sum_{i=1}^n T_i / n$  is given. The difference between the DMD and the full model (Sim.) is small. The temperature difference  $\Delta T = |T - T_{Sim}|$  between DMD and the full model, given in Fig. 4 (bottom), indicates low values compared

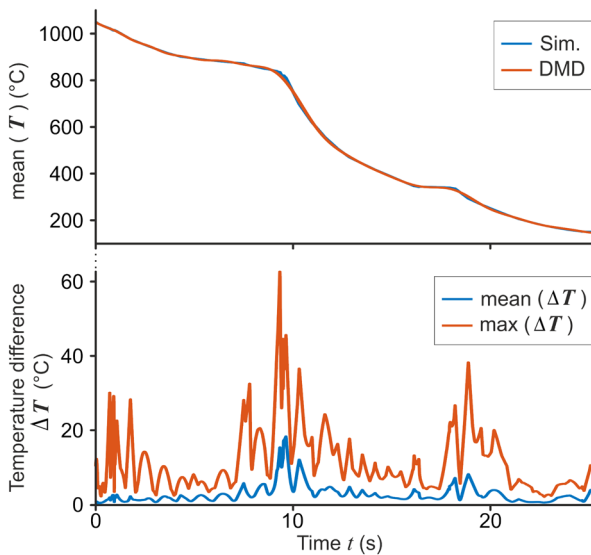


**Fig. 4** Comparison of LS-Dyna simulation results with the derived DMD model

with the absolute temperature. The average difference over all nodes  $\text{mean}(\Delta T) = \sum_{i=1}^n \Delta T_i / n$  has a maximum value of 20 °C, which occurs at the stage changes, where the knowledge of the exact temperature is not necessary for estimation during the forming process. The maximum difference over all nodes  $\text{max}(\Delta T)$  behaves similarly with higher values of up to 60 °C.

With regard to the real-time application of the models for state estimation, the respective simulation times are relevant. It is important to assess the advantage offered by the DMD model by comparing the simulation times of the process simulation with LS-Dyna and DMD. The simulation of the LS-Dyna model lasts 16 to 20 h, while the DMD model completes the simulation in just 70 ms.

### 3.2 Parametric DMD

This model generation approach needs to be extended to incorporate a parametric DMD method, allowing for different parameter configurations of the stroke rate  $f_{SR}$ , the blank holder force  $F_{BH}$ , and the austenitization temperature  $T_\gamma$ . One parametric DMD method is the stacked DMD algorithm [19]. In this method, the time series solutions for different parameter values are “stacked” to form extended snapshot matrices  $X_{1,\mu}$ , and  $X_{2,\mu}$  in Eq. (3). These matrices contain vertically stacked time series for  $N=7$  parameter realizations, represented as  $\mu = [\mu_1, \mu_2, \dots, \mu_N]^T$  for the multistage forming process. The stacked matrices are

**Table 2** Parameter sets  $\mu_i$  for  $i=1, \dots, N$

$i$	$f_{SR}$ (1/min)	$F_{BH}$ (kN)	$T_\gamma$ (°C)
1	6	20	1050
2	7	20	1050
3	8	20	1050
4	7	5	1050
5	7	40	1050
6	7	20	1000
7	7	20	1100

$$X_{1,\mu} = \begin{bmatrix} X_{1,\mu_1} \\ X_{1,\mu_2} \\ \vdots \\ X_{1,\mu_N} \end{bmatrix}, X_{2,\mu} = \begin{bmatrix} X_{2,\mu_1} \\ X_{2,\mu_2} \\ \vdots \\ X_{2,\mu_N} \end{bmatrix}, \text{ and } \phi_\mu = \begin{bmatrix} \phi_{\mu_1} \\ \phi_{\mu_2} \\ \vdots \\ \phi_{\mu_N} \end{bmatrix} \quad (3)$$

The  $N=7$  realizations, as summarized in Table 2, encompass a range of process or control variables, namely the stroke rate  $f_{SR}$ , the blank holder force  $F_{BH}$ , and the austenitization temperature  $T_\gamma$ . These variables are then combined into a tuple  $\theta = (f_{SR}, F_{BH}, T_\gamma)$ , where each element is expected to satisfy the following constraints:  $6 \text{ min}^{-1} \leq f_{SR} \leq 8 \text{ min}^{-1}$ ,  $5 \text{ kN} \leq F_{BH} \leq 40 \text{ kN}$ , and  $1000 \text{ °C} \leq T_\gamma \leq 1100 \text{ °C}$ .

The previously summarized DMD algorithm is then applied using these matrices of stacked snapshots, which yields the parametric projected DMD modes  $\Phi_\mu$  in Eq. (3). For any new parametric realization  $\theta$ , the projected DMD modes  $\Phi(\theta)$  are obtained through Lagrangian interpolation between the  $\Phi_{\mu_j}, j=1, \dots, N$  matrices. The approximate solution of the temperature distribution for any given time  $t$  is

$$T(\theta, t) \approx \Phi(\theta)e^{\Omega t}b(\theta) \quad (4)$$

The different parameter configurations lead to different temperature developments. The mean temperatures across all nodes  $\text{mean}(T)$  for five different stroke rates  $f_{SR}$  are depicted in Fig. 5 (top). The blank holder force is set to  $F_{BH}=20 \text{ kN}$ , and the austenitization temperature to  $T_\gamma=1050 \text{ °C}$ . While the temperature evolutions for  $f_{SR}=6 \text{ min}^{-1}, f_{SR}=7 \text{ min}^{-1}$ , and  $f_{SR}=8 \text{ min}^{-1}$  are obtained from the conventional DMD,  $f_{SR}=6.5 \text{ min}^{-1}$  and  $f_{SR}=7.5 \text{ min}^{-1}$  are derived by the parametric DMD using interpolation (ip.). A higher stroke rate  $f_{SR}$  speeds up the process, resulting in shorter process times  $t_e$  and higher temperatures at the end of the process.

The middle illustration of Fig. 5 shows the mean temperatures  $\text{mean}(T)$  for five different blank holder forces  $F_{BH}$  with  $f_{SR}=7 \text{ min}^{-1}$  and  $T_\gamma=1050 \text{ °C}$ .  $F_{BH}=5 \text{ kN}, F_{BH}=20 \text{ kN}$ , and  $F_{BH}=40 \text{ kN}$  are derived by conventional DMD, while  $F_{BH}=10 \text{ kN}$  and  $F_{BH}=30 \text{ kN}$  are interpolated from the parameter configurations in Table 2. A higher blank holder force  $F_{BH}$  reduces the average temperature in the stretch-forming stage. In the die-bending stage, this difference

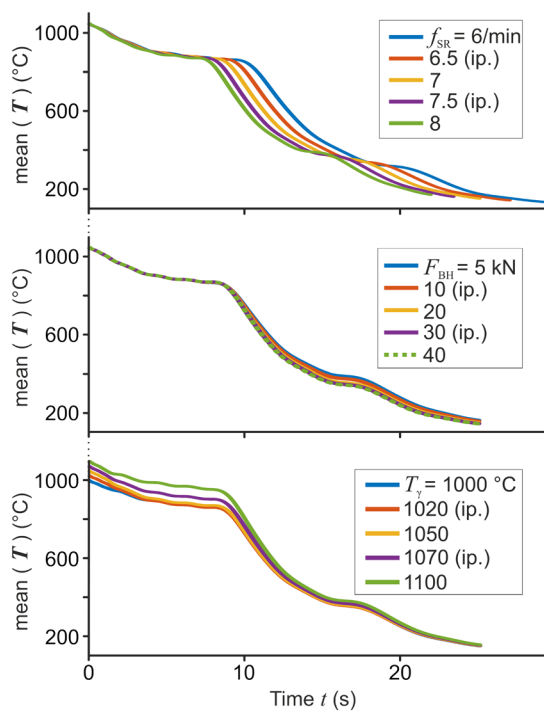


**Fig. 5** Comparison of LS-Dyna simulation results with the derived DMD model for different settings of the control variables

remains constant. Five different austenitization temperatures  $T_\gamma = 1000\text{ °C}$ ,  $T_\gamma = 1050\text{ °C}$ ,  $T_\gamma = 1100\text{ °C}$ , and the interpolated  $T_\gamma = 1025\text{ °C}$  and  $T_\gamma = 1075\text{ °C}$  are depicted in Fig. 5 (bottom). The austenitization temperature  $T_\gamma$  is the only parameter that affects the starting temperature. The difference becomes smaller as the process progresses.

To evaluate the functionality of the parametric DMD, the resulting temperature evolutions of two-parameter configurations differing from the ones used for the interpolation (see Table 2) are simulated using Eq. (4) and are compared with corresponding LS-Dyna simulations. The configuration with  $f_{SR} = 7.5\text{ min}^{-1}$ ,  $F_{BH} = 20\text{ kN}$ , and  $T_\gamma = 1050\text{ °C}$ , where the stroke rate  $f_{SR}$  differs from the originally used parameter configurations, is depicted in Fig. 6 (top). The blue line represents the temperature difference averaged across all nodes' mean ( $\Delta T$ ). It is negligibly small with maxima at the stage changes (transportation of the sheet) where the knowledge of the exact temperature is not required as discussed in Sect. 3.1. The red line represents the maximum difference  $\max(\Delta T)$ , which reaches values up to  $80\text{ °C}$ , with an average of  $30\text{ °C}$ . These differences are deemed acceptable in terms of absolute temperature. For configurations with more different parameters, the difference is also small. This is shown for  $f_{SR} = 6.5\text{ min}^{-1}$ ,  $F_{BH} = 30\text{ kN}$ , and  $T_\gamma = 1000\text{ °C}$  in Fig. 6 (bottom). The mean difference exhibits a comparable pattern to the previous configuration. However, the maximum difference is smaller during the pre-cooling stage

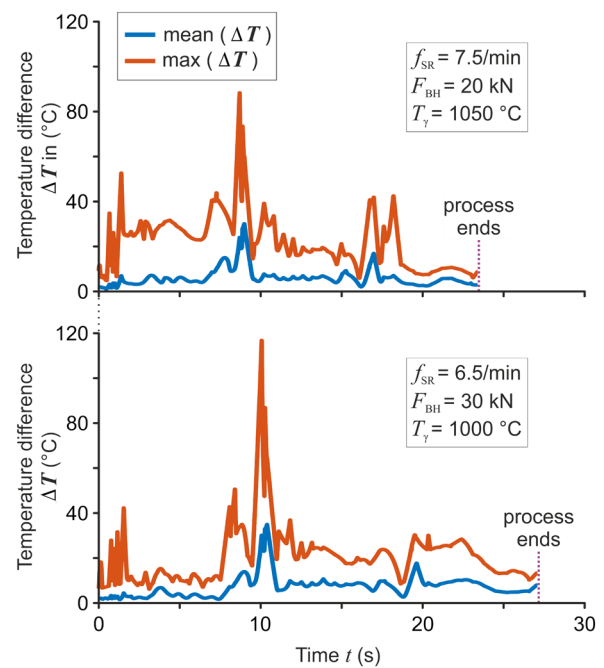


**Fig. 6** Difference between the average temperature evolutions obtained from the parametric DMD and those from LS-Dyna simulations for different  $\theta = (f_{SR}, F_{BH}, T_\gamma)$

and reaches a higher maximum during the transition to the stretch-forming stage than in the previous configuration.

### 3.3 Design of the Temperature Estimator

The parametric DMD model, combined with the temperature measurements  $y(t_k)$ , results in the discrete-time representation

$$\begin{aligned} T_r(t_{k+1}) &= A_r T_r(t_k), k \in \mathbb{N}, T_r(t_0) = T_r^0 \\ y(t_k) &= C_r(t_k) T_r(t_k) \end{aligned} \tag{5}$$

with  $T_r(\cdot) = T_r(\theta, \cdot) \in \mathbb{R}^r$  the reduced state vector and initial values  $T_r^0$  at time  $t_0 = 0\text{ s}$ . Note that the mapping  $T(\theta, t_k) = U_r T_r(\theta, t_k) \in \mathbb{R}^n$  gives the full temperature vector. The sampling time  $\Delta t = t_{k+1} - t_k = 0.01\text{ s}$  and the system matrix  $A_r(\theta) \in \mathbb{R}^{r \times r}$  are determined by the parametric DMD. The output matrix  $C(t_k) \in \mathbb{R}^{n_{sen} \times n}$  for the full-order system is stage-dependent, which can be converted into a time-varying setting given the stroke rate  $f_{SR}$ . It must be formed from the actual sensor configuration. As explained in Sect. 2, the temperature is measured by five spring-loaded thermocouples installed in die stages. Each thermocouple measures the temperature in the sheet blank in one of the three stages, while the ram is near the bottom dead center. The temperatures are read with an added thermal imaging camera and pyrometers at these positions, while the press is open. In the pre-cooling and the stretch-forming stages, the temperatures

are measured at  $n_{\text{sen}} = 2$  positions, and in the die-bending stage the temperature is measured only at  $n_{\text{sen}} = 1$  position. By applying the projection  $C_r(t_k) = C(t_k)U_r$ , the corresponding reduced output matrix for Eq. (5) is obtained.

The estimator is set up in the simulator-corrector form

$$\begin{aligned}\hat{T}(t_{k+1}) &= A_r \hat{T}_r(t_k) + L(t_k)(y(t_k) - \hat{y}(t_k)), k \in \mathbb{N}, \hat{T}_r(t_0) = \hat{T}_r^0, \\ \hat{y}(t_k) &= C_r(t_k) \hat{T}_r(t_k)\end{aligned}\quad (6)$$

In particular, a discrete-time Kalman filter is designed to minimize the variance of the estimation error  $\tilde{T}_r(t_k) = T_r(t_k) - \hat{T}_r(t_k)$  under the assumption of zero mean Gaussian process and measurement noise with covariances  $Q \in \mathbb{R}^{n \times n}$  and  $R(t_k) \in \mathbb{R}^{n_{\text{sen}} \times n_{\text{sen}}}$  [20]. The time-varying estimator gain matrix

$$L(t_k) = P(t_k)C_r(t_k)^T(C_r(t_k)P(t_k)C_r(t_k)^T + R(t_k))^{-1}$$

with the matrix  $P(t_k)$  obtained from solving the discrete-time algebraic Riccati equation

$$\begin{aligned}P(t_k) &= A_r P(t_k) A_r^T - (A_r P(t_k) C_r(t_k)^T)(R(t_k) \\ &+ C_r(t_k) P(t_k) C_r(t_k)^T)^{-1} (C_r(t_k) P(t_k) A_r^T) + Q\end{aligned}$$

In the following a comparison between the DMD model  $T(t_k)$  and the DMD-based estimator  $\hat{T}_r(t_k)$  is exemplarily evaluated for  $\theta = (8 \text{ min}^{-1}, 20 \text{ kN}, 1050 \text{ }^\circ\text{C})$ . The estimation error of the Kalman filter  $\tilde{T}_r(t_k)$  for an initial value of  $\hat{T}_r^0 = T_r^0 + 10 \text{ }^\circ\text{C} \mathbf{1}$ , i.e., an initial deviation of  $10 \text{ }^\circ\text{C}$  on all states, is depicted in Fig. 7. The average error mean ( $\tilde{T}$ ) across all nodes is small with maximums up to  $3 \text{ }^\circ\text{C}$ , while the maximum error from all nodes  $\max(\tilde{T})$  is slightly larger within an acceptable range. Both errors increase after the press is at the BDC in the stretch-forming stage as the temperature changes fast at this time point.

With the developed estimator, it becomes possible to reconstruct the spatial-temporal temperature distribution on the sheet metal  $T(\theta, t)$  for all relevant parameter configurations  $\theta$ . The error of the soft sensor emerges as the combined error of the DMD model and the Kalman filter.

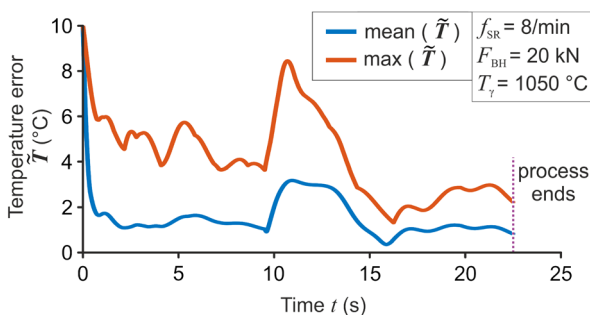


**Fig. 7** Mean estimation error over all nodes  $\text{mean}(\tilde{T})$  and maximum estimation error from all nodes  $\max(\tilde{T})$  for  $\theta = (8 \text{ min}^{-1}, 20 \text{ kN}, 1050 \text{ }^\circ\text{C})$

The temperature distribution can be estimated based on local thermocouple measurements with a total error of less than  $10 \text{ }^\circ\text{C}$  compared with the LS-Dyna simulation during the process-relevant time steps. The measurement uncertainties caused by the use of hardware sensors (thermocouple, pyrometer, thermal imaging camera), which are not specifically addressed in this paper, can be taken into account by a disturbance estimator to improve overall accuracy in an application, as demonstrated by Klöser et al. [21].

## 4 Artificial Neuronal Network-Based Soft Sensor for Microstructure Prediction

As the microstructure cannot be measured in situ with existing technologies during press hardening, it must be derived from representative measurement variables with a soft sensor for the purpose of feedback. The nonlinear development of the microstructure makes a time-efficient control-oriented description by means of analytical calculations difficult. For this reason, an artificial neural network (ANN) is built as the basis for a predictive microstructure soft sensor. The measurement variables (input) for this microstructure soft sensor are the thermal and mechanical history from the upstream soft sensors, as discussed in Sect. 2, on the basis of which the phase fractions of the final microstructure are then estimated. In the first step, a parameterization of the input variables of the ANN is developed (Sect. 4.1). Subsequently, the construction of a training database (Sect. 4.2) and the ANN (Sect. 4.3) as well as a concept validation is presented (Sect. 4.4).

### 4.1 Parameterization of Thermal and Mechanical History

Each sheet element is subjected to a thermal and mechanical history during the process, on the basis of which the final microstructure evolves. The reduced parameterization of the histories (see Fig. 8) is presented in the following. For the purpose of simplification, dependencies of the microstructure evolution on the stress state are neglected and therefore not part of the parameterization. The time sequence of the stages and the characteristic shape of the ram curve are taken into account by the parameters stroke rate  $f_{\text{SR}}$  and contact ratio  $\xi$ , which represents the ratio of the contact time  $t_{\text{co}}$  to the cycle time  $t_{\text{cy}}$ . The heating rate  $r_{\text{h,S1}}$ , the austenitizing temperature  $T_\gamma$ , and the holding time  $t_\gamma$  summarize the austenitizing conditions. The cooling after the austenitizing step is described by the step-averaged cooling rates  $r_{\text{c,S2}}$  (during pre-cooling),  $r_{\text{c,S3}}$  (during stretch-forming), and  $r_{\text{c,S4}}$  (during die-bending). To describe the mechanical history, which in the example process is limited to the forming in the third

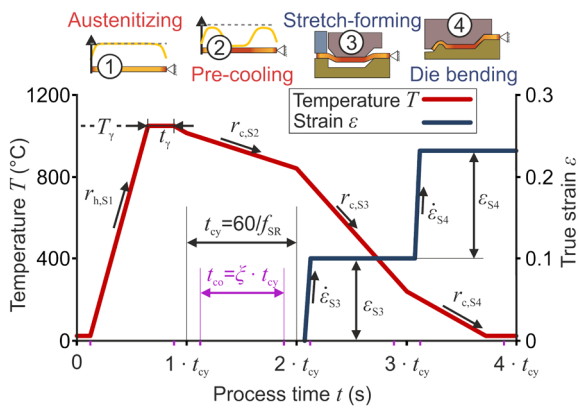


**Fig. 8** Parameterization of the thermal and mechanical history for an exemplary sheet metal element in the demo process for multi-stage press hardening

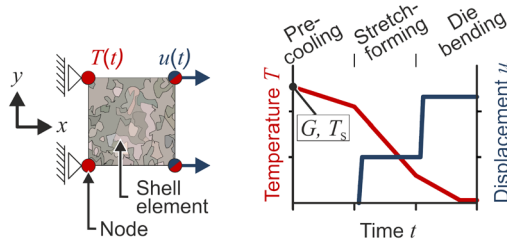


**Fig. 9** Setup of the 1-element model in LS-Dyna

and fourth stages, the true strain rate  $\dot{\epsilon}$  and the true strain  $\epsilon$  are employed. It is assumed that in each forming stage, the forming process is completed when the bottom dead center of the ram curve is reached.

### 4.2 Building a Training Database with Parametrized a 1-Element Model

To facilitate the training of the ANN, a dataset is required that establishes the correlation between different thermo-mechanical histories and the resulting microstructure, in this case, the final phase fractions  $\xi_i$ . With the aim to develop such a dataset, a 1-element model is implemented in LS-Dyna (see Fig. 9). In this model, an element undergoes the thermo-mechanical history according to the previously defined parameterization. Here, the temperature  $T$  is imposed over time  $t$  on the 4 nodes of a shell element. The austenitization stage of the process is not simulated. Instead, a homogeneous austenitic microstructure with a grain size  $G$  and a starting temperature  $T_s$  is assumed as the initial condition. Two of the nodes have their  $x$ -displacement suppressed, while the other two nodes undergo a time-dependent displacement  $u(t)$ , which induces the strain  $\epsilon$  in the element.

In the model, the evolution of the microstructure of the calculated element is captured using the material model

Mat248 (PHS\_BMW) [22]. This material model incorporates the diffusionless phase transformation from austenite to martensite, and the phase transformation by diffusion, according to implementations based on Hippchen et al. [23]. The diffusionless phase transformation is determined by various factors, as expressed in Eq. (7)). These factors include the current phase fraction of martensite  $\xi_M$  and austenite  $\xi_A$ , the current temperature  $T$  and the martensite start temperature  $M_S$ , as well as the material-dependent model parameters  $\alpha$ ,  $n$ ,  $\varphi_M$ , and  $\psi_M$ .

$$\frac{d\xi_M}{dT} = \alpha (M_S - T)^n \xi_M^{\varphi_M} (1 - \xi_M)^{\psi_M(2-\xi_A)} \quad (7)$$

The time-dependent diffusion-controlled phase transformation of the phases  $i$ , characterized by the phase fraction  $\xi_i$ , can be expressed as a function, as shown in Eq. (8). This function considers several parameters, including the phase-specific grain size parameter  $\omega_i$ , the grain size  $G$  of the austenite (specified in ASTM units), the equilibrium temperature  $T_{eq,i}$ , the current temperature  $T$ , the phase-dependent exponent  $p_i$ , the activation energy  $Q_i$  for the initiation of the diffusion–reaction, the universal gas constant  $R$ , the alloy-dependent coefficient  $c_i$ , and the transformation kinetic parameters  $c_{r,i}$ ,  $\varphi_i$ , and  $\psi_i$ .

$$\frac{d\xi_i}{dt} = 2\omega_i G (T_{eq,i} - T)^{p_i} \left( \frac{e^{\frac{Q_i}{RT}}}{c_i} \right) \left( \frac{\xi_i^{\varphi_i(1-\xi_i)} (1 - \xi_i)^{\psi_i \xi_i}}{e^{c_{r,i} \xi_i^2}} \right) \quad (8)$$

Moreover, the model considers the acceleration of phase transformations from austenite to bainite, ferrite, and pearlite, which is caused by strain introduced into the austenitic microstructure. This is achieved by scaling the activation energies of the transformations [24]. The initial grain size  $G$ , obtained after rapidly heating the material to the austenitization temperature  $T_\gamma$  with a holding time  $t_\gamma$ , is determined according to Eq. (9) [25]. The activation energy  $Q_r$ , as well as the parameters  $K$  and  $z$ , are material-dependent, empirical constants.

$$G = (K \cdot t_\gamma \cdot e^{-Q_r/(R \cdot T_\gamma)})^z \quad (9)$$

The LS-Opt program is used to systematically vary the input parameters of the 1-element model (as described in the parameterization in Sect. 4.1) implemented in LS-Dyna. This variation is carried out within the relevant parameter space and the resulting simulation data is processed to create a training data set for the ANN. Since a full factorial calculation of all possible parameter combinations would mean a considerable simulation effort, the parameter space is covered by utilizing a space-filling design of experiments with a maximized distance between each simulation point.

It should be noted that the material model presented above is used to provide a reasonable representation of the

microstructure evolution throughout the multi-stage process. However, the comprehensive validation of whether the model is fully applicable to the multi-stage process falls outside the scope of this paper. The focus here is on developing a transferable concept, where the database can be interchangeable.

### 4.3 Structure and Training of the Microstructure Soft Sensor ANN

According to the parameterization derived above, the developed ANN requires 12 input parameters defining the thermal and mechanical history. In turn, the output of the ANN provides correlation for 5 parameters, which describe the phase fractions  $\xi_i$  of the final microstructure. Specifically, these parameters represent the phase fractions of austenite  $\xi_A$ , ferrite  $\xi_F$ , pearlite  $\xi_P$ , bainite  $\xi_B$ , and martensite  $\xi_M$ .

Tensorflow is used to create ANN's structure and train it [26]. In total, the designed ANN consists of four layers. The first layer does not have any trainable parameters and is composed of 12 input parameters, which are scaled between  $-2$  and  $2$ , using the standard scaler “sklearn”. The second layer comprises 126 neurons, while the third layer consists of 64 neurons. Both of these layers employ the Rectified Linear Unit (ReLU) as the activation function, connecting the input and the output layers. The fourth layer—the output layer—consists of 5 output parameters. Here, the “Softmax” activation function is used to normalize the output, resulting in values between 0 and 1, which corresponds to phase fractions  $\xi_i$  ranging from 0 to 100%. The database generated using the 1-element model presented above consists of 3000 data sets, which are divided into 70% for training data and 30% for test data. The test data is used to evaluate the network on overfitting and, on the other hand, to validate the training progress with unfamiliar data sets. The initial values and parameters of the network are set randomly. The training process of the network employs the Adam optimizer [27]. The weights and offsets of the network are determined during the training of the ANN via error backpropagation by optimizing the mean square error. After training the ANN, the average deviation in terms of calculating a specific phase fraction is 0.084% in comparison to the training data. It should be noted that additional ANN-builds with more neurons and layers are trained and tested. However, no significant reduction of the average deviation presented above is obtained. Other activation functions have not been tested.

### 4.4 Comparison of Microstructure Soft Sensor and Full Process Simulation

For the first validation of the ANN-based microstructure soft sensor concept and the underlying parameterization, its prediction quality is checked by means of a numerical simulation

of the multi-stage press hardening process. The simulation of the multi-stage process is implemented with the FEM software LS-Dyna (see Fig. 10), using the same material modeling as in Sect. 4.2. To model the individual process stages, the basic structure follows the methodology described in Hochholdingler [22]. With values based on Shaprio [28], the heat exchange between the sheet, the tools, and the environment, as well as the yield stress and the modulus of elasticity of the 22MnB5 sheet material are modeled. The process of heating the sheet to the austenitizing temperature is not simulated. Instead, a defined temperature distribution depending on the specified austenitizing temperature is assigned to the nodes of the blank with the assumption that a homogeneous austenitic microstructure is present. Similarly, resistance heating and cooling in the pre-cooling stage of the progressive die are taken into account in a simplified way by a thermal boundary condition imposed on the nodes of the blank. From the full process simulation, the thermal and mechanical histories for representative shell elements (here of S1, S2, and S3) are evaluated and converted accordingly into the input parameters for the microstructure soft sensor. This way the input generated from the numerical simulation is used to emulate the output from the temperature and plasticity soft sensors upstream in the presented soft sensor cascade (see Fig. 1). In addition, the final phase fractions are written out from the full process simulation for the purpose of comparison with the prediction of the microstructure soft sensor. When a specific phase fraction is determined, the average percentage deviation  $\overline{PD}_{\%}$  between the prediction of the microstructure soft sensor and the full process simulation is less than 1.8% for the investigated shell elements. Furthermore, the maximum per-phase deviation in the given examples is 5.3% and occurs in the prediction of the bainite phase.

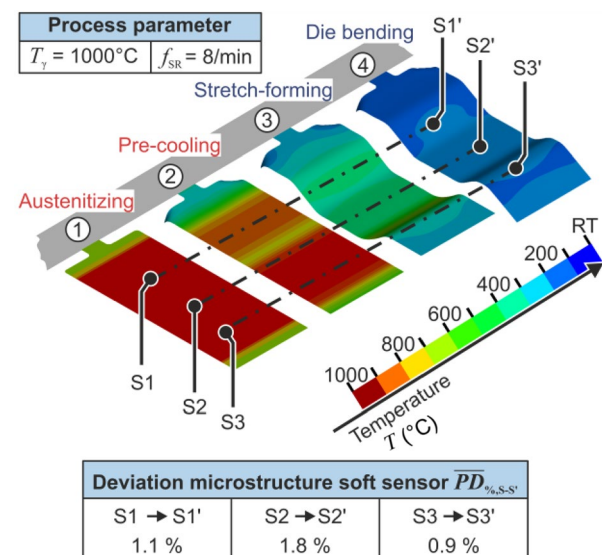


**Fig. 10** Evaluation of the microstructure soft sensor based on a full process simulation of multi-stage press hardening

this case, the calculation of the full process simulation takes 16–20 h, and the prediction for the microstructure of a shell element with the microstructure soft sensor  $< < 1$  s. The given times are achieved on a computer with Windows 10 Pro 64-bit operating system and an Intel Xeon E3-1245 processor (clock speed: 3.5 GHz).

## 5 Prediction of Product Properties

The benefit of the developed soft sensor concept is that additional modeling approaches for the prediction of several product properties can be easily implemented, modified, or replaced. In the following, examples are provided to demonstrate how different macroscopic product properties could be predicted and explicitly calculated on the basis of the DMD- and the phase fraction output of the microstructure soft sensor.

A mixing rule (Eq. (10)) could be used to estimate the hardness  $HV$  of the final microstructure, depending on the hardness of the individual phases  $HV_i$  and the phase fractions  $\xi_i$ .

$$HV = \sum_i HV_i \cdot \xi_i \quad (10)$$

From the output of the temperature soft sensor, the prediction of the hardness of the bainite fraction and thus of the entire final microstructure could be further refined by considering the cooling rate sensitivity of the bainite hardness. According to Smoljan et al. [29] the hardness of the bainite fraction  $HV_B$  can be modeled with Eq. (11).

$$HV_B = HV_{B,max} - K_{HV,B} \cdot \log\left(\frac{t_{B,8/5}}{t_{B,max}}\right) \quad (11)$$

$HV_{B,max}$  is the maximum bainite hardness, which is set within the cooling time of  $t_{B,max}$ , and  $K_{HV,B}$  is a material constant for fitting the equation.  $t_{B,8/5}$  represents the time required to cool the material from 800 °C to 500 °C and can be determined online during the multi-stage process due to the output of the above-described temperature soft sensor. In the case of 22MnB5, the hardness of the resulting ferrite, pearlite, and martensite phases is almost independent of the cooling rate and can therefore be assumed to be constant [30]. From the hardness estimated on the basis of the soft sensor output, the tensile strength  $TS$  could be determined in situ as a supplementary product property. For example, according to Löbbe et al. [31], the hardness  $HV$  of 22MnB5 can be correlated to the tensile strength with a standard deviation of 23.3 HV10 using the empirical linear Eq. 12.

$$HV = 0.325 \cdot \text{MPa}^{-1} \cdot TS + 67.9 \quad (12)$$

## 6 Conclusions

A new control method for predicting the product properties in multi-stage press hardening by utilizing soft sensors for a feedback loop is presented. First, a temperature soft sensor based on dynamic mode decomposition (DMD) is developed. This sensor can estimate the temperature (distribution) for all process-relevant control variables by extending it to a parametric DMD with an error  $< 10$  °C during the process-relevant time steps. Thus, by using a few hardware sensors that measure point-by-point or discontinuously over time, in conjunction with the temperature sensor, the entire spatial and temporal distribution of temperature can be fed back for the purpose of control. Furthermore, an artificial neural network (ANN)-based microstructure soft sensor is developed, which predicts the final phase fractions based on plasticity estimation and the output of the presented temperature soft sensor. The microstructure soft sensor can predict the final phase composition in a time span of  $< < 1$  s with an average deviation per phase of 1.8%. This allows both the hardness and the tensile strength to be determined in situ by simple correlations.

**Acknowledgements** The authors thank the German Research Foundation (DFG) for the financial support of project 424334660 in the Collaborative Research Centre SPP2183 “Property-controlled forming processes” (German: Eigenschaftsgeregelte Umformprozesse).

**Funding** Open Access funding enabled and organized by Projekt DEAL.

## Declarations

**Conflict of interest** On behalf of all the authors, the corresponding author states that there is no conflict of interest.

**Open Access** This article is licensed under a Creative Commons Attribution 4.0 International License, which permits use, sharing, adaptation, distribution and reproduction in any medium or format, as long as you give appropriate credit to the original author(s) and the source, provide a link to the Creative Commons licence, and indicate if changes were made. The images or other third party material in this article are included in the article's Creative Commons licence, unless indicated otherwise in a credit line to the material. If material is not included in the article's Creative Commons licence and your intended use is not permitted by statutory regulation or exceeds the permitted use, you will need to obtain permission directly from the copyright holder. To view a copy of this licence, visit <http://creativecommons.org/licenses/by/4.0/>.

## References

1. Belanger, P.: New Zn multistep hot stamping innovation. Presented at the 16th Great Designs in Steel Seminar, Livonia, 17 May 2017
2. Mori, K., Maeno, T., Sakagami, M., Ukai, M., Agatsuma, Y.: 2-stage progressive-die hot stamping of ultra-high strength steel

- parts using resistance heating. *Procedia Eng.* **207**, 681–686 (2017). <https://doi.org/10.1016/j.proeng.2017.10.1041>
3. Mori, K., Maeno, T., Tsuchiya, M., Nanya, T.: Inclusion of hot stamping operations in progressive-die plate forging of tailored high strength gear part. *Int. J. Adv. Manuf. Tech.* **90**, 3585–3594 (2017). <https://doi.org/10.1007/s00170-016-9705-y>
  4. Neugebauer, R., Schieck, F., Polster, S., Mosel, A., Rautenstrauch, A., Schönherr, J., Pierschel, N.: Press hardening—An innovative and challenging technology. *Arch. Civ. Mech. Eng.* **12**(2), 113–118 (2012). <https://doi.org/10.1016/j.acme.2012.04.013>
  5. Demazel, N., Laurent, H., Coër, J., Carin, M., Le Masson, P., Favero, J., Canivenc, R., Salmon-Legagneur, H.: Investigation of the progressive hot die stamping of a complex boron steel part using numerical simulations and Gleeble tests. *Int. J. Adv. Manuf. Tech.* **99**, 803–817 (2018). <https://doi.org/10.1007/s00170-018-2532-6>
  6. Allwood, J.M., Duncan, S.R., Cao, J., Groche, P., Hirt, G., Kinsey, B., Kuboki, T., Liewald, M., Sterzing, A., Tekkaya, A.E.: Closed-loop control of product properties in metal forming. *CIRP Ann. Manuf. Tech.* **65**(2), 573–596 (2016). <https://doi.org/10.1016/j.cirp.2016.06.002>
  7. Löbbbe, C., Hoppe, C., Becker, C., Tekkaya, A.E.: Closed loop springback control in progressive die bending by induction heating. *Int. J. Precis. Eng. Manuf.* **16**, 2441–2449 (2015). <https://doi.org/10.1007/s12541-015-0314-8>
  8. Löbbbe, C., Tekkaya, A.E.: Mechanisms for controlling springback and strength in heat-assisted sheet forming. *CIRP Ann. Manuf. Tech.* **67**(1), 273–276 (2018). <https://doi.org/10.1016/j.cirp.2018.04.013>
  9. Theiner, W.A., Deimel, P.: Non-destructive testing of welds with the 3MA-analyzer. *Nucl. Eng. Des.* **102**(3), 257–264 (1987). [https://doi.org/10.1016/0029-5493\(87\)90172-5](https://doi.org/10.1016/0029-5493(87)90172-5)
  10. Sturm, S.: Thermographic process monitoring in press hardening and the digitalisation into an Industry 4.0 data management system. Paper presented at the 8th Int. Conf. on hot sheet metal forming of high-performance steel, Barcelona, 30 May–2 June 2022
  11. Fortuna, L., Graziani, S., Rizzo, A., Xibilia, M.G.: *Soft sensors for monitoring and control of industrial processes*. Springer, London (2007)
  12. Bambach, M., Imran, M., Sizova, I., Buhl, J., Gerster, S., Herty, M.: A soft sensor for property control in multi-stage hot forming based on a level set formulation of grain size evolution and machine learning. *Adv. Ind. Manuf. Eng.* **2**, 100041 (2021). <https://doi.org/10.1016/j.aime.2021.100041>
  13. Stebner, S.C., Maier, D., Ismail, A., Balyan, S., Dölz, M., Lohmann, B., Volk, W., Münstermann, S.: A system identification and implementation of a soft sensor for freeform bending. *Materials* **14**(16), 4549 (2021). <https://doi.org/10.3390/ma14164549>
  14. Tekkaya, A.E., Meya, R., Löbbbe, C.: Heizvorrichtung zur Erzeugung von Joule'scher Wärme bei der Erwärmung von vorzugsweise dünnwandigen Blechteilen mittels mittelfrequenterm Strom. DE102017004935A1, 22 Nov 2018
  15. Sun, C.N., Zhang, H.H.: Microstructural evolution and quenching properties of 22MnB5 steel for hot stamping during resistance heating. *Adv. Mat. R.* **9**(5), 10901–10908 (2013). <https://doi.org/10.4028/www.scientific.net/AMR.849.75>
  16. Lafarge, R., Hütter, S., Tulke, M., Halle, T., Brosius, A.: Data based model predictive control for ring rolling. *Prod. Eng. Res. Devel.* **15**, 821–831 (2021). <https://doi.org/10.1007/s11740-021-01063-1>
  17. Kutz, J.N., Brunton, S.L., Brunton, B., Proctor, J.L.: *Dynamic mode decomposition—Data-driven modeling of complex systems*. *Soc. Ind. App. Math.* (2016). <https://doi.org/10.1137/1.9781611974508>
  18. Mamakoukas, G., Xherija, O., Murphey, T.: Memory-efficient learning of stable linear dynamical systems for prediction and control. Paper presented at the 34th conf. neural inf. proc. sys., Vancouver, Canada, December 6 - 12, 2020.
  19. Sayadi, T., Schmid, P.J., Richecoeur, F., Durox, D.: Parametrized data-driven decomposition for bifurcation analysis, with application to thermo-acoustically unstable systems. *Phy. Fluids* **27**(3), 037102 (2015). <https://doi.org/10.1063/1.4913868>
  20. Gelb, A.: *Applied optimal estimation*. The Analytic Sciences Corp, MIT Press, Cambridge (1974)
  21. Klöser, D., Martschin, J., Meurer, T., Tekkaya, A.E.: Reduced order modelling for spatial-temporal temperature and property estimation in a multi-stage hot sheet metal forming process. *Adv. Ind. Manuf. Eng.* **3**, 100055 (2021). <https://doi.org/10.1016/j.aime.2021.100055>
  22. Hochholding, B.: *Simulation des Presshärteprozesses und Vorhersage der mechanischen Bauteileigenschaften nach dem Härten*, Dissertation, ETH Zürich (2012)
  23. Hippchen, P., Lipp, A., Grass, H., Craighero, P., Fleischer, M., Merklein, M.: Modelling kinetics of phase transformation for the indirect hot stamping process to focus on car body parts with tailored properties. *J. Mater. Process. Tech.* **228**, 59–67 (2016). <https://doi.org/10.1016/j.jmatprotec.2015.01.003>
  24. Bambach, M., Buhl, J., Hart-Rawung, T., Lechner, M., Merklein, M.: Towards virtual deformation dilatometry for the design of hot stamping process. *Pro. Eng.* **207**, 1821–1826 (2017). <https://doi.org/10.1016/j.proeng.2017.10.945>
  25. Löbbbe, C.: *Temperaturunterstütztes Biegen und Wärmebehandeln in Mehrstufigen Werkzeugen*, Dissertation, TU Dortmund University (2018)
  26. Abadi, M., Barham, P., Chen, J., et al.: Tensorflow: A system for large-scale machine learning. Paper presented at the 12th USENIX Symposium on operating systems design and Implementation, Savannah, USA, 2–4 November 2016
  27. Kingma, D.P., Ba, J.: Adam: A method for stochastic optimization. *ICLR* (2015). <https://doi.org/10.48550/arXiv.1412.6980>
  28. Shapiro, A.A.: Finite element modeling of hot stamping. *Steel Res. Int.* **80**(9), 658–664 (2009). <https://doi.org/10.2374/SRI08SP065>
  29. Smoljan, B., Iljkić, D., Traven, F.: Predictions of mechanical properties of quenched and tempered steel. *J. Mech. Eng.* **56**(2), 115–126 (2010)
  30. Helmholz, R.: *Numerische Abbildung des Phasenumwandlungsverhaltens vom Mangan-Bor-Stahl 22MnB5*, Dissertation, Leibniz University Hannover (2017)
  31. Löbbbe, C., Hering, O., Hiegemann, L., Tekkaya, A.E.: Setting mechanical properties of high strength steels for rapid hot forming processes. *Materials* **9**(4), 229 (2016). <https://doi.org/10.3390/ma9040229>



**Juri Martschin** Since 2018, Juri Martschin has been conducting research at the Institute of Forming Technology and Lightweight Components, TU Dortmund University, as a research associate. He has been involved in the priority program SPP2183 of the German research association (DFG) since 2020, which investigates property-controlled forming processes. His research topics cover press hardening in progressive dies in conjunction with the closed-loop control of

product properties, as well as hot shear cutting and profile bending with stress superposition.



**Malte Wrobel** is research associate at the Digital Process Engineering Group of the Karlsruhe Institute of Technology (KIT). He received the M.Sc. degree from Kiel University in Germany in Electrical Engineering, Information Technology and Business Management in 2019. Thereafter he started working as a research associate at the Automation and Control Group of the same university until February 2023. He has been involved in the priority program SPP2183 of the German research association (DFG)

since 2022, which investigates property-controlled forming processes. His current research interests are the model- and data-based temperature estimation and control design, optimal sensor placement and model order reduction.



**Joshua Grodotzki** Since 2016, Joshua Grodotzki has been conducting research at the Institute of Forming Technology and Lightweight Components, TU Dortmund University, on topics related to the digitalization of engineering education. This includes remote labs as well as digital learning tools in the areas of web, app as well as VR/AR developments. As of 2022, he is head of the research department on sheet metal and profile forming. Current work includes research topics on press hardening,

damage in forming technology and material characterization processes.



**Thomas Meurer** received the diploma in Process Systems Engineering and the Ph.D. (Dr.-Ing.) from the University of Stuttgart, Germany in 2001 and 2005, respectively. From 2005 to 2007 he was Postdoc at the Saarland University, Germany. In 2007 he became Senior Researcher at the TU Vienna, Austria and was appointed Associate Professor (Privatdozent) in 2012. From 2012 to 2023 he was Full Professor for Automation and Control at Kiel University, Germany. Since February 2023

has been Full Professor for Digital Process Engineering for Sustainable Materials and Energie at the Karlsruhe Institute of Technologie (KIT), Germany. His research interests include control of nonlinear and distributed parameter systems, observer design, multi-agent systems, and optimal control with applications in production processes, process systems engineering, robotics, and marine systems.



**A. Erman Tekkaya** is professor at TU Dortmund University in Dortmund/Germany and director of the Institute of Forming Technology and Lightweight Components (IUL). He studied mechanical engineering in Ankara/Turkey and completed his doctoral studies in Stuttgart/Germany. His research interests cover fundamentals and technology of novel metal forming processes as well as material characterization for modelling plastic deformations. He is visiting professor at the Ohio State University/USA and honorary professor at the Xi'an University/China. Prof. Tekkaya is fellow of the International Academy for Production Engineering (CIRP) and editor of *Advances in Industrial and Manufacturing Engineering* (AIME).

University/USA and honorary professor at the Xi'an University/China. Prof. Tekkaya is fellow of the International Academy for Production Engineering (CIRP) and editor of *Advances in Industrial and Manufacturing Engineering* (AIME).